Convection in rotating non-uniformly stratified spherical fluid shells in dependence on Ekman and Prandtl numbers

Ján Šimkanin, Pavel Hejda, Dana Saxonbergová-Jankovičová

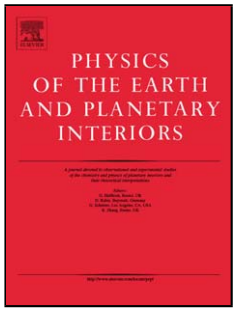

Title: Convection in rotating non-uniformly stratified spherical fluid shells in dependence on Ekman and Prandtl numbers

Authors: Ján Šimkanin, Pavel Hejda, Dana Saxonbergová-Jankovičová

PII: S0031-9201(09)00220-9
DOI: doi:10.1016/j.pepi.2009.10.010
Reference: PEPI 5218

To appear in: *Physics of the Earth and Planetary Interiors*

Received date: 19-12-2008
Revised date: 22-10-2009
Accepted date: 26-10-2009

Please cite this article as: Šimkanin, J., Hejda, P., Saxonbergová-Jankovičová, D., Convection in rotating non-uniformly stratified spherical fluid shells in dependence on Ekman and Prandtl numbers, *Physics of the Earth and Planetary Interiors* (2008), doi:10.1016/j.pepi.2009.10.010

Convection in rotating non-uniformly stratified spherical fluid shells in dependence on Ekman and Prandtl numbers

Ján Šimkanin[a*] jano@ig.cas.cz, Pavel Hejda[a] ph@ig.cas.cz, Dana Saxonbergová-Jankovičová[b] dja@ufa.cas.cz

[a]Institute of Geophysics, Academy of Sciences of the Czech Republic, Boční II/1401, 141 31 Prague, Czech Republic
[b]Institute of Atmospheric Physics, Academy of Sciences of the Czech Republic, Boční II/1401, 141 31 Prague, Czech Republic
Tel.: 420267103342
fax: 420272761549

Abstract
We present an investigation of rotating convection in non-uniformly stratified spherical shells in dependence on Prandtl, Ekman and Rayleigh numbers. Attention is focused on the case in which the thickness of both sublayers (stable and unstable) is identical, which was not investigated before. Influence of stratification is more evident at small values of Rayleigh numbers (large values of Ekman numbers), at large Rayleigh numbers is almost negligible. For small Rayleigh numbers in the case of uniform stratification a large-scale columnar convection is developed in the whole volume, in the case of non-uniform stratification it is suppressed to the unstably stratified region but slightly penetrates to the stably stratified one, except the case of large Prandtl numbers when the convection significantly penetrate to the stably stratified region. The spiralling nature of convection is a dominant feature at moderate Prandtl numbers, the strong spiralling is typical at small Prandtl numbers but it disappears at large Prandtl numbers. For large Rayleigh numbers (small values of Ekm developed. The multilayer convection (``teleconvection'') is not developed in our case of non-uniform stratification because of the significant amount of stable stratification. Our case is a typical extreme case. It is dissimilar to both cases if the stably stratified sublayer is thinner than the unstably stratified one and if the unstably stratified sublayer is thinner than the stably stratified one.

Keywords
rotating convection; non-uniform stratification; penetrative convection; small-scale structures

1 Introduction

The Earth's and planetary fluid interiors are characterized by convective motions. Convection (magnetoconvection) constitutes the driving mechanism of hydromagnetic processes leading to magnetic field generation [15]. Buoyancy, the fundamental source of convection or magnetoconvection [11], results from the complicated processes going on in the Earth's and planetary fluid interiors, e.g., a chemical homogenisation, gravitational differentiation, solidification processes acting on the inner core boundary (e.g., the convection in the mushy layer due to the mentioned solidification processes, see [9]), etc. Consequently, the outer liquid Earth's core and the liquid interiors of Giant planets are non-uniformly stratified (this means density stratification, see [8, 24]).

In general, it is assumed that the upper part of the outer liquid Earth's core (close to the core-mantle boundary[1]) is stably stratified (subadiabatic radial temperature gradient) and the lower part (towards the inner core boundary[2]) unstably stratified (superadiabatic radial temperature gradient). The idea of "a stably stratified ocean" at the top of the outer Earth's core was firstly introduced by [1]. Models of a non-uniformly stratified fluid shell are an acceptable simplification of the real Earth-like conditions. In the Earth's core the stably stratified sublayer is probably very thin (the outer Earth's core is almost unstably stratified, see [1, 8, 24, 16, 17, 21]). Such a stratification is probably typical for the terrestrial planets [24, 20, 21]. However, in the other planets the ratio of the thickness of the appropriate sublayers (e.g., of the stably stratified to unstably stratified sublayers) and their geometric configuration vary. This is noticeable especially with the Giant planets [19, 20, 24, 21].

Non-uniform stratification can be simulated thermodynamically also in the Boussinesq models by means of internal heat sources [24, 16, 17]. If the stably stratified sublayer is very thin (for a geometric configuration stable/unstable), then behaviour is close to the case of uniform stratification when the whole layer is unstably stratified. Likewise, if the unstably stratified sublayer is very thin, then behaviour is close to the case of uniform stratification when the whole layer is stably stratified. Thus, the effects of non-uniform stratification are noticeable if the thicknesses of the stably and unstably stratified sublayers are comparable [24, 16, 17, 18].

The study of hydromagnetic dynamo action in Mercury provides another good example of the influence of a stably stratified sublayer [6]. Mercury is characterized by a weak magnetic field. A possible explanation could be given by a hydromagnetic dynamo working in the similar geometric configuration as in our study (stable/unstable) but in this case a larger fraction of spherical shell is stably stratified [6]. In such a case the (magneto)convection and the dynamo action are strongly suppressed in the upper stably stratified sublayer, i.e. magneto(convection) and dynamo run in the small unstably stratified sublayer (close to ICB). Such weak dynamo action and skin-effect (the magnetic field generated in the unstably stratified sublayer permeates through the stably stratified

[1] hereinafter referred to as CMB
[2] hereinafter referred to as ICB

sublayer where it is damped due to skin-effect) lead to the weak magnetic field observed on the surface of Mercury [6].

For a different geometric configuration the influence of a non-uniform stratification is fundamental [19, 20]. They assumed reverse stratification, i.e. the stably stratified sublayer is surrounded by the unstably stratified one. This configuration leads to non-dipolar and non-axisymmetric magnetic fields, which are typical e.g., for Uranus and Neptune.

The case, in which the thickness of both sublayers is the same, was not investigated in previous studies (e.g., [24, 16, 17, 18]). Consequently, we located the change of the sign to the middle of the convective shell. A convection in rotating non-uniformly stratified spherical fluid shells was studied in dependence on Prandtl, Ekman and Rayleigh numbers. The model and governing equations are given in Section 2. The numerical results are presented in Section 3. Finally, Section 4 provides the conclusions.

2 Governing equations and model

Convection (with the velocity $\mathbf{V}$) of incompressible fluid in the Boussinesq approximation in a non-uniformly stratified spherical shell ($r_i < r < r_o$) rotating with angular velocity Ω is described by the system of dimensionless equations:

$$E\left(\frac{\partial \mathbf{V}}{\partial t} + (\mathbf{V}\cdot\nabla)\,\mathbf{V} - \nabla^2\mathbf{V}\right) + 2\mathbf{1}_z \times \mathbf{V} + \nabla P = R_a \frac{\mathbf{r}}{r_o} T, \tag{1}$$

$$\frac{\partial T}{\partial t} + (\mathbf{V}\cdot\nabla)\,T = \frac{1}{P_r}\nabla^2 T + H, \tag{2}$$

$$\nabla\cdot\mathbf{V} = 0. \tag{3}$$

The radius of the outer sphere L, is the typical length scale, which makes the dimensionless radius $r_o = 1$; the inner core radius r_i is, similar to that of the Earth, equal to 0.35. (r, θ, φ) is the spherical system of coordinates, $\mathbf{1}_z$ is the unit vector. The typical time, t, is measured in the unit of L^2/ν, typical velocity, $\mathbf{V}$, in ν/L, temperature, T, in ΔT, and pressure, P, $\rho\nu^2/L^2$. The dimensionless parameters appearing in Eqs (1)-(3) are the Prandtl number, $P_r = \nu/\kappa$, the Ekman number, $E = \nu/\Omega L^2$ and the modified Rayleigh number $R_a = \alpha g_0 \Delta T L/\Omega\nu$, where κ is thermal diffusivity, ν is kinematic viscosity, ρ is density, α is the coefficient of thermal expansion, ΔT is the drop of temperature through the shell and g_0 is the gravity acceleration at $r = r_o$.

Eqs (1)-(3) are closed by the non-penetrating and no-slip boundary conditions for the velocity field at the rigid surfaces and fixed temperature boundary conditions.

The last term in Eq. (2), H, constitutes the internal heat sources (it is the non-dimensional volumetric heat source strength), which enable simulating thermodynamically the various stratification of the spherical shells also in the Boussinesq models. The outer sphere was assumed to be stratified non-uniformly (it is divided into stably and unstably stratified sub-shells) with constant temperature $T_i = 1$ and $T_o = 0$ at the inner and outer boundaries of the

shell, respectively. The width of both sub-shells was considered the same, i.e. $\partial T/\partial r$ changes its sign in the middle of the convective shell, $r_m = (r_i + r_o)/2$. It is accomplished if $H = -23P_r^{-1}$. Let us describe why we used this value. The non-uniform stratification is considered due to internal heat sources and in the basic state Eq. (2) gets the form

$$\frac{1}{P_r}\nabla^2 T + H = 0. \tag{4}$$

If we solve Eq. (4) considering $T_i = 1$, $T_o = 0$ and $\partial T/\partial r = 0$ at $r = r_m$, we obtain $H = -23P_r^{-1}$.

3 Numerical results

Eqs (1)-(3) were solved using the MAG dynamo code [12, 13, 14, 4, 5, 7]. It is a serial version of Gary Glatzmaier's rotating spherical convection/magnetoconvection/dynamo code, modified by Ulrich Christensen and Peter Olson. The code solves the non-dimensional Boussinesq equations for time-dependent thermal convection in a rotating spherical shell filled with an electrically conducting fluid. MAG uses toroidal-poloidal decomposition for velocity and magnetic field with explicit time steps. Linear terms are evaluated spectrally (spherical harmonics plus Chebyshev polynomials in radius) and nonlinear terms are evaluated on a spherical grid (for more details, see [12, 13, 14, 4, 5, 7]). The computations were performed on the Sun Grid Engine (LUNA) at the Institute of Physics, Academy of Sciences of CR, Prague; the Nemo cluster (SGI) and PC clusters at the Institute of Geophysics, Academy of Sciences of CR, Prague.

Dependence of solutions on various values of the Prandtl number, P_r, the Ekman number, E, and the Rayleigh number, R_a, was investigated. Computations started from zero initial velocity and were performed for $P_r = 10^{-1}$, 1, 10; $E = 10^{-3}, 10^{-5}$, and $R_a = 250, 600$ (for $E = 10^{-3}$) and $R_a = 5000, 15000$ (for $E = 10^{-5}$). The Prandtl number, the ratio of the thermal diffusion time to the viscous one, is the most significant dynamic factor in our study. According to the value of P_r, it is possible to split the solutions to three qualitatively different groups, i.e. convection at low Prandtl numbers, $P_r = 1$ and large Prandtl numbers.

3.1 Prandtl number $P_r = 1$

Let us start with the most used value of P_r. In the case of $P_r = 1$ the characteristic thermal diffusion time is equal to the characteristic viscous diffusion time ($\tau_\kappa = \tau_\nu$), i.e. thermal and viscous diffusion processes equally affect the dynamics of convection. Dependence of the mean kinetic energy, E_k, on R_a, E and the type of stratification (uniform and non-uniform) for $P_r = 1$ is given in Fig. 1. In the case of uniform stratification the whole shell is unstably stratified.

E_k increases for given E with increasing of R_a and also increases with a decreasing of E (the last one is given by the increasing of the critical Rayleigh

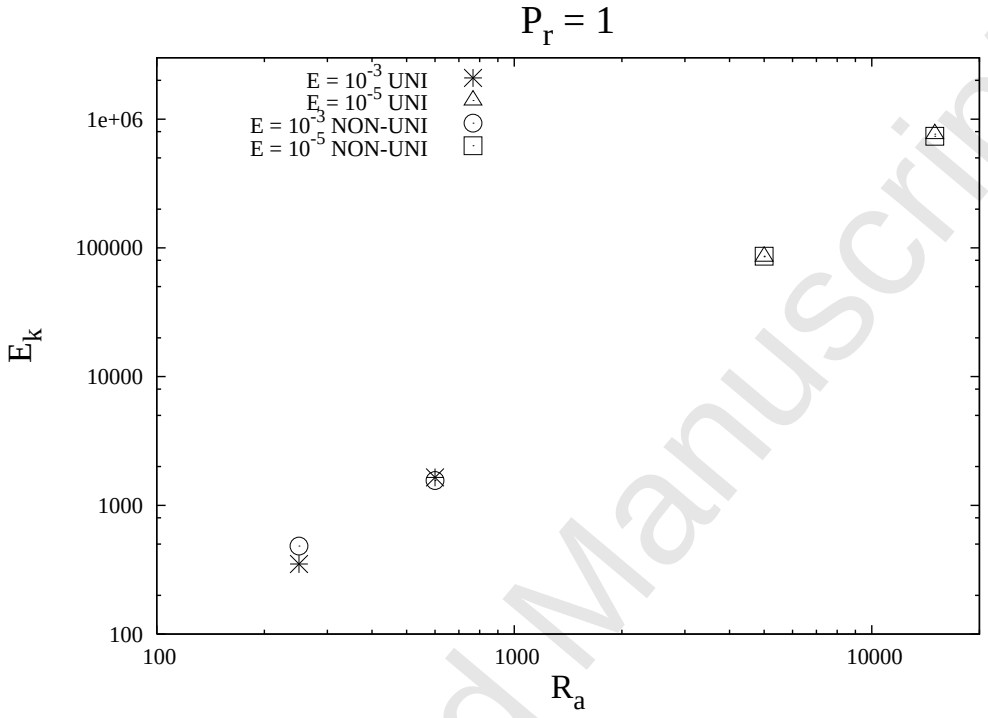

Figure 1: Dependence of the mean kinetic energy, E_k, on the Rayleigh number, R_a, the Ekman number, E, and the type of stratification (uniform - UNI and non-uniform - NON-UNI) for $P_r = 1$.

number, R_c, with decreasing of E). The dependence of E_k on the type of stratification is weak, almost negligible (see Fig. 1).

The typical space distributions of the radial velocity field component, V_r are presented in Fig. 2, Z-vorticity in Fig. 3 (equatorial sections) and the azimuthal velocity field component, V_φ in Fig. 4 (axi-symmetrical meridional sections). All the figures are snapshots done at time $t = 3.5$ (3.5 time units). Fig. 2 (and the corresponding Figs. (6) and (10)) were done using the value of $r = 0.69$ which lies in the stable region but close to the interface $r = r_m$ ($r_m = 0.675$). Consequently, we used the value of r practically equal to r_m. Dependence on the type of stratification is now more evident than of E_k (see Figs. (2-4)). It is more visible for small values of R_a (large values of E), for large values of R_a (small values of E) is almost negligible. For small values of R_a in the case of uniform stratification, a large-scale columnar convection is developed in the whole volume, while in the case of non-uniform stratification it is suppressed to the unstably stratified region but slightly penetrates to the

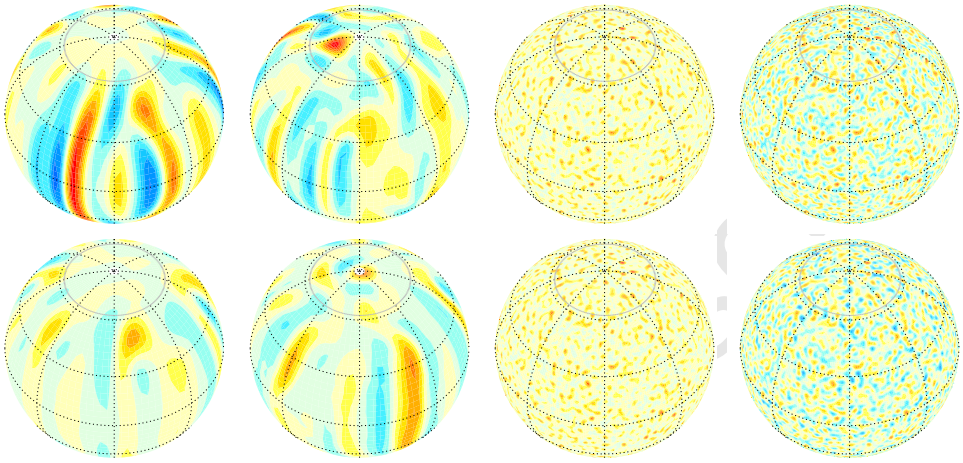

Figure 2: Space distributions of radial velocity field components V_r at $r = 0.69$ for the cases of uniform (top) and non-uniform (bottom) stratification, and for $R_a = 250, 600$ (both for $E = 10^{-3}$), $R_a = 5000, 15000$ (both for $E = 10^{-5}$) and $P_r = 1$ (from left to right). Red (blue) colours indicate positive (negative) values. Minimal and maximal values for the first line are (-48, 48), (-136, 136), (-261, 261), (-791, 791), and for the second line (-78, 78), (-173, 173), (-296, 296), (-905, 905). Snapshots at $t = 3.5$.

stably stratified one (see Figs. (2-3)). This behaviour is known from previous analyses [24, 16, 17, 3]. Increasing R_a it is possible to observe a transition from the large-scale convection to the small-scale convection (Figs. (2-4) from left to right). The vorticity is the much larger in the cases of high Rayleigh numbers (see Fig. 3). For $E = 10^{-5}$ and $R_a = 5000, 15000$ only a small-scale convection is developed.

The spiralling cross section of the columns as a dominant feature at moderate Prandtl numbers, causes the Reynolds stress whose action generates a differential rotation, i.e. the spiralling cross section of the columns causes a differential rotation [3, 22]. This feature, observable for small values of R_a, is in our case for large values of R_a unseen. Some irregularities in the spiralling structure of columnar convection could be probably caused by the differential rotation, so-called "active" and "quiet" zones [3]. Let us briefly comment our lack of columnar structures at lower values of E, when for similar values of the Rayleigh numbers, a convection at $E = 10^{-5}$ would be much more columnar than convection at $E = 10^{-3}$. Our values of R_a are very large in the case of $E = 10^{-5}$, so large that the effect of rotation is scarcely visible (buoyancy forces are much stronger than Coriolis forces). This is apparent in Fig. 2. Plots of a

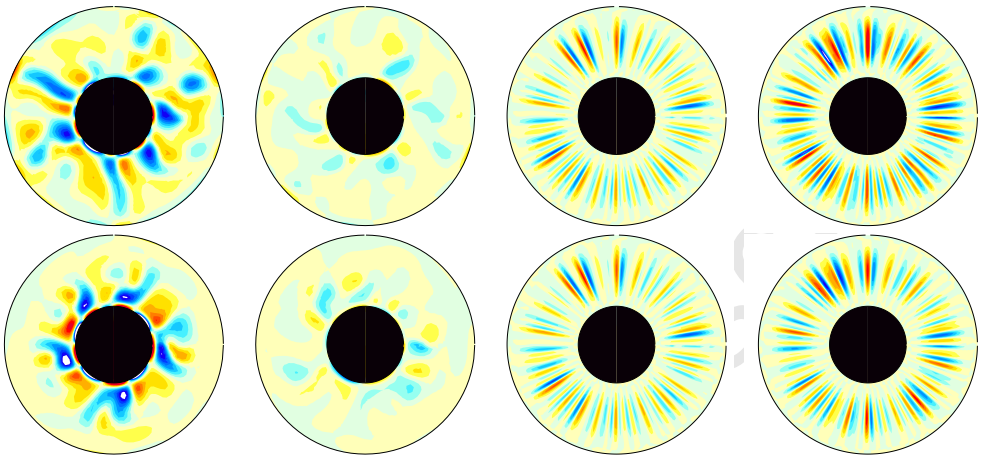

Figure 3: Equatorial sections of Z-vorticity for the cases of uniform (top) and non-uniform (bottom) stratification, and for $R_a = 250, 600$ (both for $E = 10^{-3}$), $R_a = 5000, 15000$ (both for $E = 10^{-5}$) and $P_r = 1$ (from left to right). Red (blue) colours indicate positive (negative) values. Minimal and maximal values for the first line are (-108, 108), (-115, 115), (-349, 349), (-864, 864), and for the second line (-113, 113), (-123, 123), (-401, 401), (-957, 957). Snapshots at $t = 3.5$.

meridional cross-section of the radial velocity (not axi-symmetric just any section) would make it clearer whether the convection has a columnar structure or not.

The multilayer convection ("teleconvection") is not developed in our case of non-uniform stratification because of the significant amount of stable stratification. An excitation of toroidal motions in the outermost part of the shell ("teleconvection") is a consequence of the radial stratification, without which they cannot take place, and is possible if the unstable stratification dominates over the stable one [24, 3].

3.2 Low Prandtl numbers

In the case of low Prandtl numbers ($P_r < 1$) the characteristic thermal diffusion time is smaller than the characteristic viscous diffusion time ($\tau_\kappa < \tau_\nu$), i.e. thermal diffusion processes dominate over viscous ones. Inertial modes become important (see left side of Eq. (1), where the inertial term is not negligible in comparison with the viscous one). The main difference between convection at $P = 10^{-1}$ (we put $P = 10^{-1}$ in the case of low Prandtl numbers) and $P = 1$ occurs at the transition between regular and irregular patterns [2]. Dependence of the mean kinetic energy, E_k, on R_a, E and the type of stratification (uniform

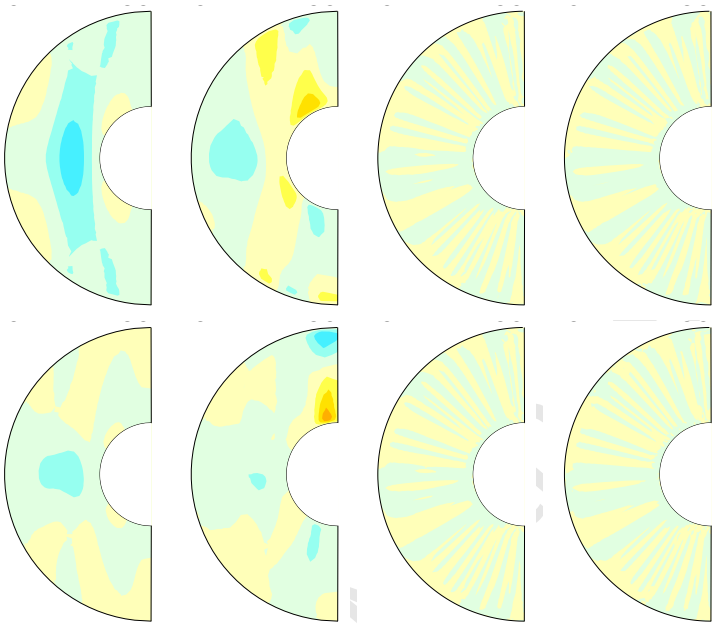

Figure 4: Axi-symmetrical meridional sections of azimuthal velocity field components V_φ for the cases of uniform (top) and non-uniform (bottom) stratification, and for $R_a = 250, 600$ (both for $E = 10^{-3}$), $R_a = 5000, 15000$ (both for $E = 10^{-5}$) and $P_r = 1$ (from left to right). Red (blue) colours indicate positive (negative) values. Minimal and maximal values for the first line are (-18, 18), (-47, 47), (-89, 89), (-264, 264), and for the second line (-27, 27), (-61, 61), (-96, 96), (-304, 304). Snapshots at $t = 3.5$.

and non-uniform) for $P_r = 10^{-1}$ is given in Fig. 5.

E_k again increases for given E with increasing of R_a and also increases with a decreasing of E. The dependence of E_k on the type of stratification is again weak, almost negligible, but for $E = 10^{-5}$ and $R_a = 15000$ is strong (see Fig. 5).

The typical space distributions of the radial velocity field component, V_r are presented in Fig. 6, Z-vorticity in Fig. 7 (equatorial sections) and the azimuthal velocity field component, V_φ in Fig. 8 (axi-symmetrical meridional sections). All the figures are snapshots done at time $t = 3.5$. Dependence on the type of stratification is now again more evident than of E_k (see Figs. (6-8)). For $R_a = 250$ (left columns) and $R_a = 15000$ (right columns) it is strong (except for the radial component of velocity, V_r, displayed in Fig. 6 where it is weak). In the case of uniform stratification for $R_a = 250$ a large-scale columnar convection with the strong spiralling nature is developed in the whole

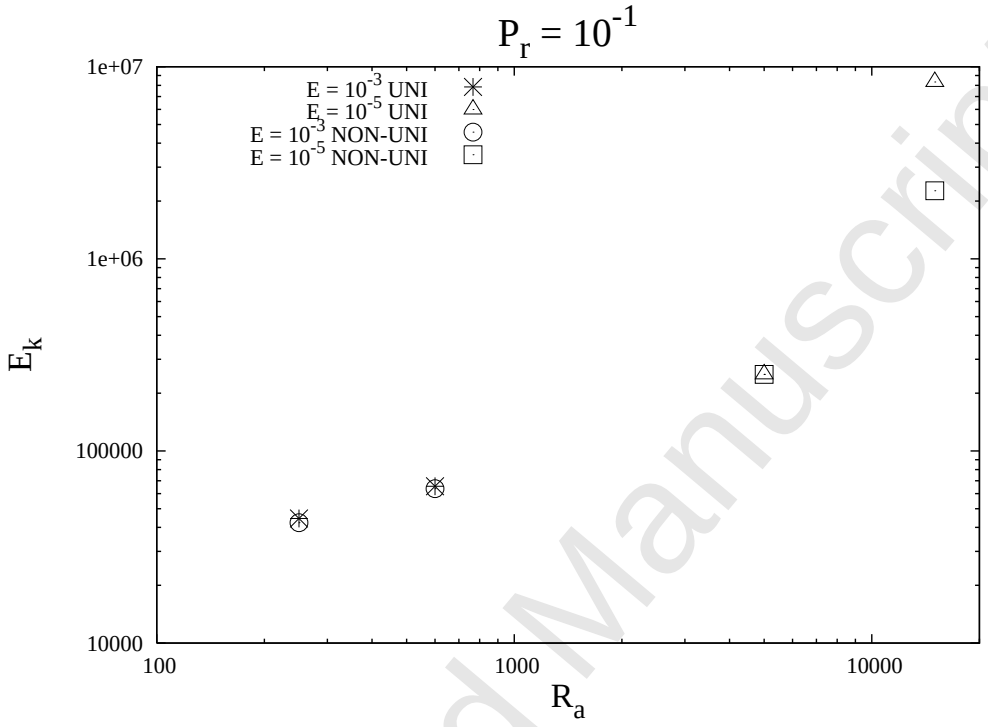

Figure 5: Dependence of the mean kinetic energy, E_k, on the Rayleigh number, R_a, the Ekman number, E, and the type of stratification (uniform - UNI and non-uniform - NON-UNI) for $P_r = 10^{-1}$.

volume, in the case of non-uniform stratification it is again suppressed to the unstably stratified region (shifted out from CMB) but slightly penetrates to the stably stratified one (see Figs. (6-7)). The spiralling character of a columnar convection causes a differential rotation [2, 22]. For $R_a = 15000$ it is possible to observe a small-scale convection without a strong spiralling because this value of R_a is far more strongly supercritical, and buoyancy forces are much stronger than Coriolis forces.

3.3 Large Prandtl numbers

In the case of large Prandtl numbers ($P_r > 1$) the characteristic thermal diffusion time is greater than the characteristic viscous diffusion time ($\tau_\kappa > \tau_\nu$), i.e. viscous diffusion processes dominate over thermal ones. The typical difference between convection at $P_r = 1$ and $P_r = 10$ (we put $P = 10$ in the case of large Prandtl numbers) is that the convection columns retain their alignment

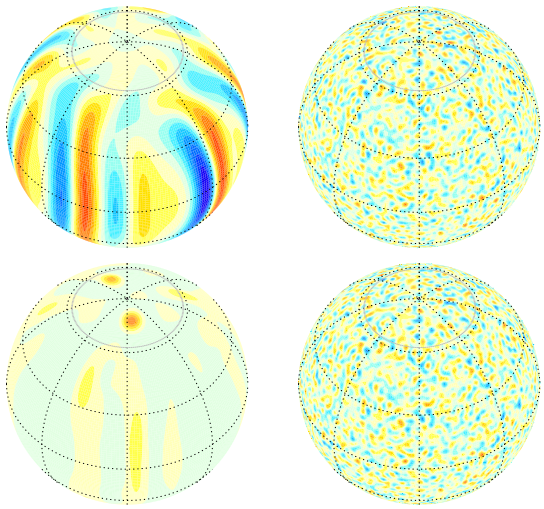

Figure 6: Space distributions of radial velocity field components V_r at $r = 0.69$ for the cases of uniform (top) and non-uniform (bottom) stratification, and for $R_a = 250$ (for $E = 10^{-3}$), $R_a = 15000$ (for $E = 10^{-5}$) and $P_r = 10^{-1}$ (from left to right). Red (blue) colours indicate positive (negative) values. Minimal and maximal values for the first line are (-807, 807), (-2621, 2621), and for the second line (-779, 779), (-1440, 1440). Snapshots at $t = 3.5$.

with the axis of rotation with increasing P_r, but the spiralling nature of their radial orientation disappears [3]. As P_r increases the influence of the differential rotation, which dominates the evolution of the convection columns for P_r of the order unity and bellow diminishes rapidly [3].

As in previous cases E_k increases for given E with increasing of R_a but its increasing with a decreasing of E is not so strong as for $P_r = 1$ and $P_r < 1$. The dependence of E_k on the type of stratification is strong for $E = 10^{-3}$ but for $E = 10^{-5}$ it is weak, almost negligible (see Fig. 9).

The typical space distributions of the radial velocity field component, V_r are presented in Fig. 10, Z-vorticity in Fig. 11 (equatorial sections) and the azimuthal velocity field component, V_φ in Fig. 12 (axi-symmetrical meridional sections). All the figures are snapshots done at time $t = 3.5$. Dependence on the type of stratification is now again more evident than of E_k (see Figs. (10-12)). For $R_a = 250$ (left columns) it is strong but for $R_a = 15000$ (right columns) it is weak (except for the azimuthal component of velocity, V_φ, displayed in Fig. 12 where it is strong). For $R_a = 250$ a convection is developed in the whole volume in the both cases of uniform and non-uniform stratifications. It is interesting that in the case of non-uniform stratification the convection significantly penetrates to the stably stratified region (it is not suppressed to the unstably

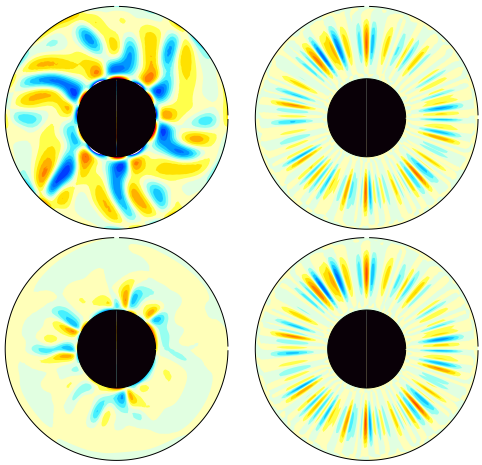

Figure 7: Equatorial sections of Z-vorticity for the cases of uniform (top) and non-uniform (bottom) stratification, and for $R_a = 250$ (for $E = 10^{-3}$), $R_a = 15000$ (for $E = 10^{-5}$) and $P_r = 10^{-1}$ (from left to right). Red (blue) colours indicate positive (negative) values. Minimal and maximal values for the first line are (-1203, 1203), (-4095, 4095), and for the second line (-1128, 1128), (-2114, 2114). Snapshots at $t = 3.5$.

stratified one as it is typical for $P_r = 1$ and $P_r < 1$, see Figs. (11), (3), (7)). For $R_a = 15000$ it is possible to observe a small-scale-convection (similarly as in previous cases). The azimuthal flow is generally weaker at high values of P_r than low ones (see Figs. (4), (8), (12)).

4 Conclusions

A density stratification plays a significant role in the astrophysical and geophysical processes. It is an important dynamical factor in the processes acting in planetary atmospheres (e.g., [10]), planetary interiors (e.g., [1, 19, 20, 24, 21, 6, 16, 17]), etc.

A systematical parameter study of rotating convection in uniformly and non-uniformly stratified spherical shells in dependence on Prandtl, Ekman and Rayleigh numbers was done e.g., in [24, 2, 3]. Our attention is focused on the case when the thickness of both sublayers (stable and unstable) is the same. Such a case was not investigated in previous studies (e.g., [23, 24, 16, 17, 18]). It is true that neither planet nor satellite with this geometric configuration has been observed. Nevertheless, it is interesting to investigate such a case in order to answer a question whether its behaviour is closer to the case of a stable stratification or an unstable one. Thus, we investigate our model in dependence

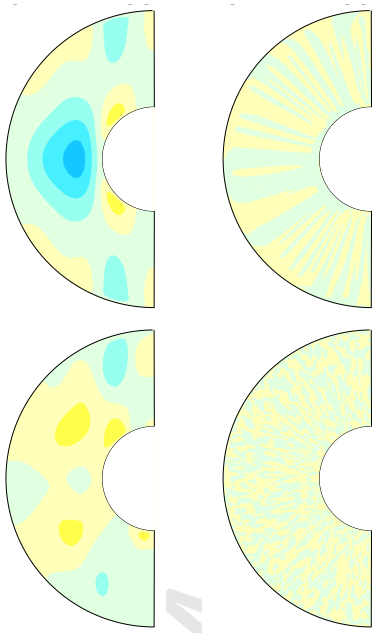

Figure 8: Axi-symmetrical meridional sections of azimuthal velocity field components V_φ for the cases of uniform (top) and non-uniform (bottom) stratification, and for $R_a = 250$ (for $E = 10^{-3}$), $R_a = 15000$ (for $E = 10^{-5}$) and $P_r = 10^{-1}$ (from left to right). Red (blue) colours indicate positive (negative) values. Minimal and maximal values for the first line are (-271, 271), (-876, 876), and for the second line (-262, 262), (-485, 485). Snapshots at $t = 3.5$.

on Prandtl, Ekman and Rayleigh numbers, and the type of stratification (in order to compare an influence of a non-uniform stratification, we investigated also the case of an unstably stratified shell).

The Prandtl number is the most significant dynamic factor in our study. Consequently, we split the solutions to three qualitatively different groups, i.e. convection at low, moderate and large Prandtl numbers. The mean kinetic energy, E_k, increases for given E with increasing of R_a and also increases with a decreasing of E (the last one is given by the increasing of the critical Rayleigh number, R_c, with decreasing of E). The dependence of E_k on the type of stratification is weak, almost negligible except the cases of $E = 10^{-5}$, $R_a = 15000$ for $P_r = 10^{-1}$ and $E = 10^{-3}$ for $P_r = 10$ when it is strong (see Figs. (1), (5), (9)). Dependence on the type of stratification is more evident on the typical space distributions of the velocity field and vorticity, mainly for small values of R_a (large values of E). For large values of R_a (small values of E) is almost negligible. For small values of R_a in the case of uniform stratification a

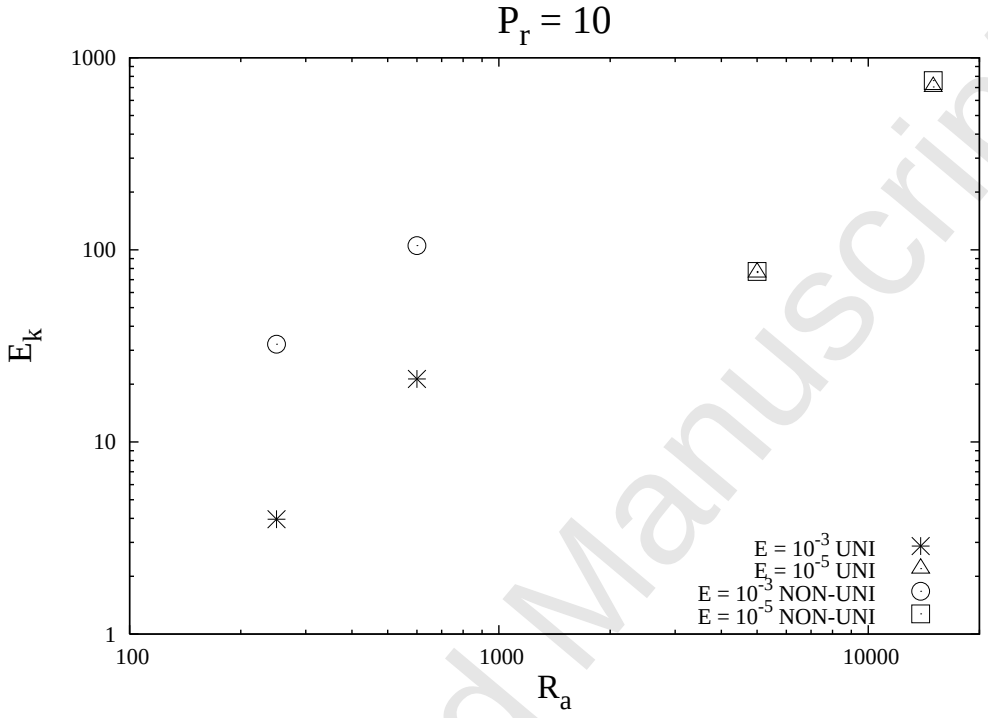

Figure 9: Dependence of the mean kinetic energy, E_k, on the Rayleigh number, R_a, the Ekman number, E, and the type of stratification (uniform - UNI and non-uniform - NON-UNI) for $P_r = 10$.

large-scale columnar convection is developed in the whole volume, in the case of non-uniform stratification it is suppressed to the unstably stratified region but slightly penetrates to the stably stratified one, except the case of $P_r = 10$ when the convection significantly penetrates to the stably stratified region (it is not suppressed to the unstably stratified one). The vorticity is the much larger in the cases of high Rayleigh numbers for all P_r (see Figs. (3), (7), (11)). The azimuthal flow is generally weaker at high values of P_r than low ones (see Figs. (4), (8), (12)). The spiralling cross section of the columns which causes a differential rotation, is a dominant feature at $P_r = 1$ and becomes stronger at $P_r = 10^{-1}$, but it disappears at $P_r = 10$. For large values of R_a (small values of E) only a small-scale convection is developed (it is possible to observe small-scale structures). However, it is necessary to remark again that our values of R_a for $E = 10^{-5}$ are far more strongly supercritical, and buoyancy forces are much stronger than Coriolis forces (the effect of rotation is scarcely visible). This is apparent in Figs. (2) and (6), where the results for $E = 10^{-5}$ have no columnar

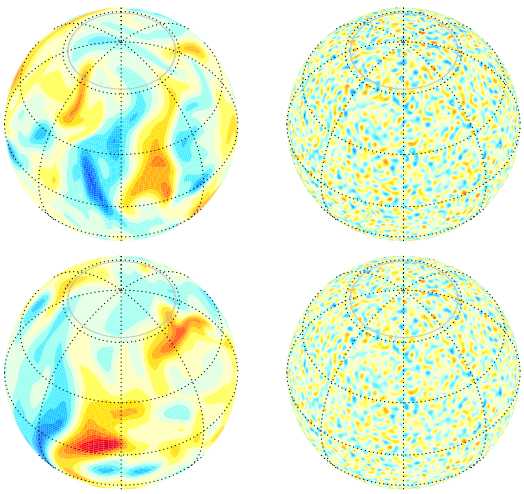

Figure 10: Space distributions of radial velocity field components V_r at $r = 0.69$ for the cases of uniform (top) and non-uniform (bottom) stratification, and for $R_a = 250$ (for $E = 10^{-3}$), $R_a = 15000$ (for $E = 10^{-5}$) and $P_r = 10$ (from left to right). Red (blue) colours indicate positive (negative) values. Minimal and maximal values for the first line are (-5.5, 5.5), (-38, 38), and for the second line (-14, 14), (-42, 42). Snapshots at $t = 3.5$.

structure, but instead resemble non-rotating convection, e.g., no spiralling even at low P_r (which is characterized by strong spiralling) in the rightmost figures of Figs. (3) and (7). Consequently, the plots of a meridional cross-section of the radial velocity would make it clearer whether the convection has a columnar structure or not.

The multilayer convection ("teleconvection") is not developed in our case of non-uniform stratification because of the significant amount of stable stratification.

Our results are in agreement with previous analyses done in the uniformly (e.g., [2]) or non-uniformly stratified spherical shells (e.g., [23, 24, 16, 17, 18, 3]). The convective motions were qualitatively described in [23, 24, 3], etc. We showed that the case characterized by the identical thicknesses of both sublayers is a typical extreme case. It is dissimilar to the case if the stably stratified sublayer is thinner than the unstably stratified one (although the convection penetrates to the stably stratified sublayer, it is more suppressed to the unstably stratified sublayer than in the case if r_m is closer CMB) and also dissimilar to the case when the unstably stratified sublayer is thinner than the stably stratified one (although the convection is significantly suppressed to the unstably stratified sublayer, still penetrates to the stably stratified sublayer more than in the case

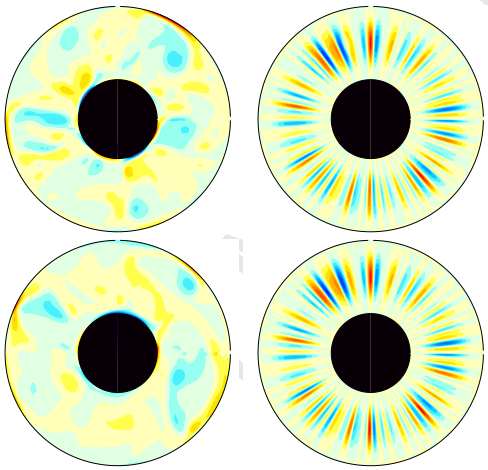

Figure 11: Equatorial sections of Z-vorticity for the cases of uniform (top) and non-uniform (bottom) stratification, and for $R_a = 250$ (for $E = 10^{-3}$), $R_a = 15000$ (for $E = 10^{-5}$) and $P_r = 10$ (from left to right). Red (blue) colours indicate positive (negative) values. Minimal and maximal values for the first line are (-8.3, 8.3), (-54, 54), and for the second line (-21, 21), (-65, 65). Snapshots at $t = 3.5$.

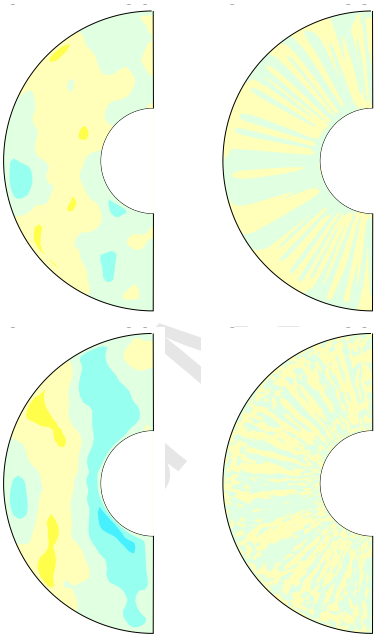

Figure 12: Axi-symmetrical meridional sections of azimuthal velocity field components V_φ for the cases of uniform (top) and non-uniform (bottom) stratification, and for $R_a = 250$ (for $E = 10^{-3}$), $R_a = 15000$ (for $E = 10^{-5}$) and $P_r = 10$ (from left to right). Red (blue) colours indicate positive (negative) values. Minimal and maximal values for the first line are (-2.05, 2.05), (-12.71, 12.71), and for the second line (-4.61, 4.61), (-14.23, 14.23). Snapshots at $t = 3.5$.

if r_m is closer ICB).

Acknowledgements

This research has been supported by the Grant Agency of the Academy of Sciences of the Czech Republic (Grant No. IAA300120704). We would like to thank G. Glatzmaier, U. Christensen, P. Olson, and CIG for MAG dynamo code, and the Institute of Physics of Academy of Sciences of CR, Prague for CPU time on the Sun Grid Engine (the Luna project). Our thanks includes also two unknown referees, whose comments greatly improved this paper.

References

[1] Braginsky, S., 1964. Magnetohydrodynamics of the Earth's Core. Geomagn. Aeron. 4, 898–916 (Engl. Transl. 698–712).

[2] Busse, F.H., Simitev, R., 2005. Convection in rotating spherical fluid shells and its dynamo states. In: Soward, A.M., Jones, C.A., Hughes, D.W., Weiss, N.O. (Eds.), Fluid Dynamics and Dynamos in Astrophysics and Geophysics, 359–392, CRC Press, New York, USA.

[3] Busse, F.H., Simitev, R., 2007. 3.4. Convection in rotating spherical fluid shells. In: Soward, A.M., Dromy, E. (Eds.), Mathematical Aspects of Natural Dynamos, 168–198, CRC Press, New York, USA.

[4] Christensen, U.R., Olson, P., Glatzmaier, G.A., 1999. Numerical modelling of the geodynamo: a systematic parameter study. Gephys. J. Int. 138, 393–409.

[5] Christensen, U.R., Aubert, J., Cardin, P., Dormy, E., Gibbons, S., Glatzmaier, G.A., Grote, E., Honkura, Y., Jones, C., Kono, M., Matsushima, M., Sakuraba, A., Takahashi, F., Tilgner, A., Wicht, J., Zhang, K., 2001. A numerical dynamo benchmark. Phys. Earth Planet. Inter. 128, 25–34.

[6] Christensen, U.R., 2006. A deep dynamo generating Mercury's magnetic field. Nature 444, 1056–1058. doi:10.1038/nature05342

[7] Christensen, U.R., Aubert, J., 2006. Scaling properties of convection drivne dynamos in rotating spherical shells and application to planetary magnetic fields. Geophys. J. Int. 166, 97–114.

[8] Fearn, D.R., Loper, D.E., 1981. Compositional convection and stratification of the Earth's core. Nature 289, 393–394.

[9] Guba, P., Worster, M.G., 2006. Nonlinear oscillatory convection in mushy layers. J. Fluid Mech. 553, 419–443.

[10] Heimpel, M., Aurnou, J., Wicht, J., 2005. Simulation of equatorial and high-latitude jets on Jupiter in a deep convection model. Nature 438, 193–196. doi:10.1038/nature04208

[11] Jones, C.A., 2000. Convection-driven geodynamo models. Phil. Trans. R. Soc. Lond. A 358, 873–897.

[12] Olson, P., Glatzmaier, G.A., 1993. Highly supercritical thermal convection in a rotating spherical shell: centrifugal vs. radial gravity. Geophys. Astrophys. Fluid Dyn. 70, 113–136.

[13] Olson, P., Glatzmaier, G.A., 1995. Magnetoconvection in a rotating spherical shell: structure of flow in the outer core. Phys. Earth Planet Int. 92, 109–118.

[14] Olson, P., Glatzmaier, G.A., 1996. Magnetoconvection and thermal coupling of the Earth's core and mantle. Phil. Trans. R. Soc. Lond. A354, 1413–1424.

[15] Roberts, P.H., Glatzmaier, G.A., 2000. Geodynamo theory and simulations. Rev. Mod. Phys. 72 (4), 1081–1123.

[16] Šimkanin, J., Brestenský, J., Ševčík, S., 2003. Problem of the rotating magnetoconvection in variously stratified fluid layer revisited. Stud. Geophys. Geod. 47, 827–845.

[17] Šimkanin, J., Brestenský, J., Ševčík, S., 2006. On hydromagnetic instabilities and the mean electromotive force in a non-uniformly stratified Earth's core affected by viscosity. Stud. Geophys. Geod. 50, 645–661.

[18] Šimkanin, J., 2008. Control volume method for hydromagnetic dynamos in non-uniformly stratified spherical shells. Contributions to Geophysics and Geodesy 38 (1), 1–15.

[19] Stanley, S., Bloxham, J., 2004. Convective-region geometry as the cause of Uranus' and Neptune's unusual magnetic fields. Nature 428, 151–153.

[20] Stanley, S., Bloxham, J., 2006. Numerical dynamo models of Uranus' and Neptune's magnetic fields. Icarus 184, 556–572.

[21] Stanley, S., Mohammadi, A., 2008. Effects of an outer thin stably stratified layer on planetary dynamos. Phys. Earth Planet. Inter. 168, 179–190.

[22] Zhang, K., 1992. Spiralling columnar convection in rapidly rotating spherical fluid shells . J. Fluid Mech, 236, 535–556.

[23] Zhang, K., 1994. On coupling between the Poincare equation and the heat-equation. J. Fluid Mech, 268, 211–229.

[24] Zhang, K., Schubert, G., 2000. Teleconvection: remotely driven thermal convection in rotating stratified spherical layers. Science, 290, 1944–1947.